



Validation of GOSAT
XCO₂ using aircraft
measurement

M. Inoue et al.

This discussion paper is/has been under review for the journal Atmospheric Chemistry and Physics (ACP). Please refer to the corresponding final paper in ACP if available.

Validation of XCO₂ derived from SWIR spectra of GOSAT TANSO-FTS with aircraft measurement data

M. Inoue¹, I. Morino¹, O. Uchino¹, Y. Miyamoto², Y. Yoshida¹, T. Yokota¹, T. Machida¹, Y. Sawa³, H. Matsueda³, C. Sweeney⁴, P. P. Tans⁴, A. E. Andrews⁴, and P. K. Patra⁵

¹National Institute for Environmental Studies (NIES), Tsukuba, Japan

²Graduate School of Natural Science and Technology, Okayama University, Okayama, Japan

³Meteorological Research Institute (MRI), Tsukuba, Japan

⁴National Oceanic and Atmospheric Administration (NOAA), Boulder, CO, USA

⁵Research Institute for Global Change, JAMSTEC, Yokohama, Japan

Received: 30 November 2012 – Accepted: 21 January 2013 – Published: 4 February 2013

Correspondence to: M. Inoue (inoue.makoto@nies.go.jp)

Published by Copernicus Publications on behalf of the European Geosciences Union.

Title Page

Abstract

Introduction

Conclusions

References

Tables

Figures



Back

Close

Full Screen / Esc

Printer-friendly Version

Interactive Discussion



Abstract

Column-averaged volume mixing ratios of carbon dioxide (XCO_2) retrieved from Greenhouse gases Observing SATellite (GOSAT) Short-Wavelength InfraRed (SWIR) observations were compared with aircraft measurements by the Comprehensive Observation Network for TRace gases by AirLiner (CONTRAIL) project, the National Oceanic and Atmospheric Administration (NOAA), and the National Institute for Environmental Studies (NIES). Before validation, we investigated the impacts of GOSAT SWIR column averaging kernels (CAK) and the shape of a priori profiles on the calculation of XCO_2 based on aircraft measurements (aircraft-based XCO_2). The differences between aircraft-based XCO_2 with and without the application of GOSAT CAK were evaluated to be less than ± 0.4 ppm at most, and less than 0.1 ppm on average. Therefore, we concluded that the GOSAT CAK produces only a minor effect on the aircraft-based XCO_2 calculation in terms of the overall uncertainty of GOSAT XCO_2 .

In this study, two approaches were used to validate GOSAT products (Ver. 02.00). First, we performed a comparison of GOSAT data retrieved within ± 2 -degree or ± 5 -degree latitude/longitude boxes centered at each aircraft measurement site and aircraft-based data measured on a GOSAT overpass day (i.e. extraction of temporally matched cases). As this method resulted in no matched data for observation sites where no aircraft measurement was made on the GOSAT overpass day, we also attempted to validate GOSAT products by gap-filling the aircraft-based XCO_2 time series through curve fitting. Both methods indicated that GOSAT XCO_2 agreed well with aircraft-based XCO_2 , except that the former is negatively biased by 1–2 ppm with a standard deviation of 1–3 ppm.

1 Introduction

Global warming has become a serious international environmental issue over the last few decades. Forecasting concentrations of carbon dioxide (CO_2) which is the most

ACPD

13, 3203–3246, 2013

Validation of GOSAT XCO_2 using aircraft measurement

M. Inoue et al.

Title Page

Abstract

Introduction

Conclusions

References

Tables

Figures

◀

▶

◀

▶

Back

Close

Full Screen / Esc

Printer-friendly Version

Interactive Discussion



Validation of GOSAT XCO₂ using aircraft measurement

M. Inoue et al.

Title Page

Abstract

Introduction

Conclusions

References

Tables

Figures

◀

▶

◀

▶

Back

Close

Full Screen / Esc

Printer-friendly Version

Interactive Discussion



important anthropogenic greenhouse gas (GHG) is required to predict the magnitude of global warming and future climate conditions. Atmospheric CO₂ concentrations have been measured with high accuracy at ground stations, tall towers, ships, aircraft, and balloons using flask sampling or continuous measurement equipment. These measurements have provided extensive information regarding the latitudinal distribution and temporal variations of CO₂ in the atmosphere (e.g. Pales and Keeling, 1965; Conway et al., 1988; Komhyr et al., 1989; Tans et al., 1989; Inoue and Matsueda, 1996; Nakazawa et al., 1997b; Watanabe et al., 2000; Matsueda et al., 2002; Machida et al., 2008; Sawa et al., 2008). Atmospheric measurements have also provided reasonable estimates of the global land-ocean partitioning or latitudinal distributions of surface fluxes of CO₂ through inverse modeling (Enting, 2002). However, because of the sparseness of existing observation sites and the limitations of their altitudinal range, current estimates of regional CO₂ sources and sinks have large uncertainties (Gurney et al., 2002).

Recently, a great deal of attention has been given to CO₂ observations using satellite remote sensing technology that can identify the regional distribution of GHGs and estimate their emissions and absorptions at the sub-continental scale. Rayner and O'Brien (2001) reported that the uncertainty in CO₂ fluxes estimated by inverse modeling can be substantially reduced if the current surface network is supplemented by space-borne measurements of CO₂ column averaged concentrations provided that individual column concentrations achieved a precision within 1%. Compared to the conventional measurements made by ground stations and aircraft noted above, GHG observations by satellites have an advantage that the whole globe can be observed by a single instrument. In general, however, satellite observation is considered to be less accurate than ground-based measurement (e.g. Christi and Stephens, 2004). Therefore, satellite-based data products must be validated by higher-precision data obtained independently using atmospheric measurements at the Earth's surface or on board the aircraft.

Validation of GOSAT XCO₂ using aircraft measurement

M. Inoue et al.

Title Page

Abstract

Introduction

Conclusions

References

Tables

Figures

◀

▶

◀

▶

Back

Close

Full Screen / Esc

Printer-friendly Version

Interactive Discussion

Here, we present a brief overview of the current situation regarding GHG observations using satellite remote sensing. Chédin et al. (2002) reported that annual trends and seasonal variations of CO₂ concentrations can be obtained by processing the spectral data derived from High-Resolution Infrared Sounder (HIRS) onboard the National Oceanic and Atmospheric Administration (NOAA) polar meteorological satellites. Crevoisier et al. (2004) showed that seasonal cycles and the latitudinal dependence of CO₂ concentrations in the mid-troposphere, derived from Thermal InfraRed (TIR) spectra of the Atmospheric Infrared Sounder (AIRS) onboard the Aqua satellite platform of the National Aeronautics and Space Administration (NASA), agree well with those made by aircraft observations. The SCanning Imaging Absorption SpectroMeter for Atmospheric Cartography (SCIAMACHY) instrument onboard ENVISAT, launched in March 2002, makes nadir observations in the near-infrared of the main greenhouse gases and the ozone precursor gases (Dils et al., 2006). Column-averaged volume mixing ratios of carbon dioxide (XCO₂) derived from the SCIAMACHY instrument have been compared to data from ground-based Fourier Transformed Spectrometers (ground-based FTS) (Dils et al., 2006; Schneising et al., 2012; Heymann et al., 2012).

More recently, the Greenhouse gases Observing SATellite “IBUKI” (GOSAT), the world’s first satellite dedicated to measuring the atmospheric concentrations of CO₂ and CH₄ from space has been operated since the early 2009 and the preliminary results have been published by the National Institute for Environmental Studies (NIES) GOSAT project team (Yokota et al., 2009; Yoshida et al., 2011; Morino et al., 2011). Yoshida et al. (2011) presented global distributions of XCO₂ and column-averaged volume mixing ratios of methane (XCH₄) retrieved from the Short-Wavelength InfraRed (SWIR) spectra of the Thermal And Near-infrared Sensor for carbon Observation – Fourier Transform Spectrometer (TANSO-FTS) onboard the GOSAT. Morino et al. (2011) performed the preliminary validation of GOSAT SWIR XCO₂ and XCH₄ (Ver. 01.xx, earlier version released in August 2010) using data provided by a worldwide network of ground-based FTS called the Total Carbon Column Observing Network

(TCCON; Wunch et al., 2011). The results indicated that Ver. 01.xx of the GOSAT SWIR XCO₂ was biased by 8.85 ± 4.75 ppm ($2.3\% \pm 1.2\%$) lower than the reference values.

In this study, Ver. 02.00 of the GOSAT SWIR XCO₂ (released in June 2012) was validated using aircraft measurement vertical data. As satellite observations are not equally sensitive to all atmospheric layers, aircraft measurement data must be weighted with the GOSAT SWIR column averaging kernels (CAK, see Sect. 3.1.4) when calculating XCO₂. It is necessary to apply the GOSAT SWIR CAK and convolution with the a priori profiles used in satellite data retrievals to the aircraft measurement data for a meaningful comparison between the two measurements. The column-averaged volume mixing ratios weighted with the CAK of spectroscopic remote sensing such as satellite and ground-based high-resolution FTS are often calculated when comparing with in situ data or global model simulations (e.g. Buchwitz et al., 2005; Schneising et al., 2008; Saito et al., 2012). However, in this study, XCO₂ based on aircraft measurements (aircraft-based XCO₂) had to be converted to temporally continuous data by curve fitting (Nakazawa et al., 1997a; Miyamoto et al., 2012) over locations where there were no GOSAT data, and then aircraft-based XCO₂ was temporally matched for the whole period (see Sect. 4). In such cases, it is very difficult to apply GOSAT SWIR CAK to temporally interpolated aircraft-based XCO₂ (see Sect. 3.1.4). Therefore, we first evaluated the impact of the GOSAT SWIR CAK on the aircraft-based XCO₂ calculation. Aircraft-based XCO₂ without the application of GOSAT SWIR CAK was compared to aircraft-based XCO₂ weighted with the GOSAT SWIR CAK. Based on the results, the aircraft-based XCO₂ was used for validation of the GOSAT SWIR XCO₂.

This paper is organized as follows: in Sect. 2, we describe GOSAT products, the aircraft measurements and meteorological tower data used in this study. In Sect. 3, the methodology used for the analysis is provided. In Sect. 4, the impacts of GOSAT SWIR CAK and assumed profiles in the stratosphere and mesosphere on aircraft-based XCO₂ calculation are examined. Then, comparisons between GOSAT products and aircraft-based XCO₂ are performed. We conclude the paper with a summary in Sect. 5.

Validation of GOSAT XCO₂ using aircraft measurement

M. Inoue et al.

Title Page

Abstract

Introduction

Conclusions

References

Tables

Figures

⏪

⏩

◀

▶

Back

Close

Full Screen / Esc

Printer-friendly Version

Interactive Discussion



2 Observations

2.1 Overview of GOSAT and products retrieved from GOSAT TANSO-FTS SWIR spectra

GOSAT was launched on 23 January 2009 from the Japan Aerospace Exploration Agency (JAXA) Tanegashima Space Center in Japan and has been operational since April 2009. GOSAT flies at an altitude of approximately 666 km and completes one revolution in about 100 min. The satellite returns to the same point in space in 3 days making global observations of several tens of thousands of ground points by TANSO-FTS. TANSO-FTS has three SWIR spectral bands centered at 0.76, 1.6, and 2.0 μm and one broad TIR band between 5.6 and 14.3 μm . XCO_2 and CO_2 concentration profile can be retrieved from SWIR and TIR bands, respectively (Saitoh et al., 2009; Yoshida et al., 2011). This study focuses on validation of XCO_2 retrieved from SWIR spectra by the latest retrieval algorithm (Ver. 02.xx; Yoshida et al., 2013). From all SWIR spectra observed with TANSO-FTS, the cloud-free measurements with solar zenith angle less than 70° and signal-to-noise ratio (SNR) larger than 70 for O_2 sub-band (12 950–13 200 cm^{-1}) are selected and used to retrieve XCO_2 . After the quality check for the retrieved results, the typical range of the XCO_2 a posteriori error is 0.8–1.4 ppm with its mode value of 0.9 ppm.

Validation of the GOSAT TANSO-FTS SWIR Level 2 products is of great significance, because these data form the basis of Level 3 (data on the global distribution of column abundances) and Level 4 products (GHG fluxes). Level 2 products are already in use as part of the observational data to estimate surface CO_2 fluxes by inverse modeling and data assimilation (e.g. Takagi et al., 2011). Therefore, GOSAT Level 2 products (Ver. 02.00 released in June 2012) must be evaluated using independent data with higher precision and no significant bias, i.e. a small degree of uncertainty. Here, we compare the GOSAT SWIR XCO_2 with aircraft-based XCO_2 .

Validation of GOSAT XCO_2 using aircraft measurement

M. Inoue et al.

Title Page

Abstract

Introduction

Conclusions

References

Tables

Figures



Back

Close

Full Screen / Esc

Printer-friendly Version

Interactive Discussion



2.2 Aircraft measurement data

The CONTRAIL project has been observing vertical CO₂ profiles using Japan Airlines Corporation (JAL) commercial airliners (Machida et al., 2008; Matsueda et al., 2008), which record frequent and spatially dense observation data. Five JAL commercial aircraft were instrumented with Continuous CO₂ Measuring Equipment (CME), and most flights originate from Narita International Airport (hereinafter, Narita) in Chiba, Japan. The data observed during the ascent and descent of the aircraft are taken as vertical CO₂ profiles over each observation site (airports) and have an overall uncertainty of 0.2 ppm. Typical observing altitudes are 1–11 km with vertical resolutions of 30–100 m. The CONTRAIL data are being used to gain an understanding of the meridional and seasonal variations of CO₂ near the tropopause (Sawa et al., 2008) and to validate or estimate CO₂ fluxes by inverse modeling for Asian regions (Patra et al., 2011; Niwa et al., 2012). The vertical CO₂ profiles are used in this study.

The NOAA Earth System Research Laboratory/Global Monitoring Division (ESRL/GMD) operates an aircraft-based flask air sampling network designed to monitor the global distribution and interannual variations of CO₂ and several other trace gases in the atmosphere (NOAA/ESRL Carbon Cycle Greenhouse Gases Aircraft Program). Several atmospheric gases, including CO₂, are measured using aircraft at about 20 sites, covering an altitude range of ~ 500 m to 7 km with vertical resolutions of 300–700 m, at weekly or biweekly sampling intervals. The measurement uncertainty is reported to be ~ 0.15 ppm. The NOAA ESRL/GMD aircraft measurements have been used for the validation of AIRS CO₂ retrieval at various pressure levels (Maddy et al., 2008).

NIES also measures CO₂ densities by flask air sampling using aircraft to examine vertical and horizontal distributions of GHGs. There are three sites in Siberia and one site in Japan. Sampling frequency is once or twice a month. Typical observing altitudes are 0.5–7 km with vertical resolutions of 0.5–1.5 km and the uncertainty of

Validation of GOSAT XCO₂ using aircraft measurement

M. Inoue et al.

Title Page

Abstract

Introduction

Conclusions

References

Tables

Figures



Back

Close

Full Screen / Esc

Printer-friendly Version

Interactive Discussion



measurements is estimated to be 0.2 ppm, including the scale difference between standard gases (Nakazawa et al., 1997c; Machida et al., 2001).

In this study, 20 CONTRAIL sites, 17 NOAA sites, and 4 NIES sites were used for validation of GOSAT products. The respective locations are shown in Fig. 1, and their basic information is given in Table 1. CONTRAIL sites are widely distributed around the world, including Asia, Oceania, and Europe, whereas NOAA sites are concentrated mainly in North America (Fig. 1).

2.3 Tower data

The aircraft measurement data are obtained over a limited altitude range (about 0.5–12 km above the surface). As for additional information below the low-boundary of the aircraft data, we use the CO₂ concentration data measured by the tall towers of the Meteorological Research Institute (MRI) and NOAA. Because there are tall towers at limited aircraft measurement sites, three aircraft sites can use tower data; NRT uses MRI tower data and LEF and WBI use NOAA tower data (see Table 1 for site code of aircraft sites).

CO₂ concentrations were observed at a meteorological tower in the MRI, Tsukuba, Japan (36.1° N, 140.1° E; Inoue and Matsueda, 1996, 2001). Atmospheric concentrations of CO₂ at altitudes of 1.5, 25, 100, and 200 m above the ground were continuously observed with a precision better than 0.1 ppm using a Non-Dispersive InfraRed (NDIR) analyzer (Inoue and Matsueda, 1996) and recorded as hourly data. The tower data nearest to the aircraft measurement time were selected to complement CO₂ profiles.

The NOAA GMD/ESRL tall tower network also provides representative measurements of CO₂ in the continental boundary layer (Andrews et al., 2011). CO₂ data from two NOAA tower sites, Park Falls (Wisconsin, USA) and West Branch (Iowa, USA), were used for LEF and WBI, respectively. There are three main observation stages: 30, 122, and 396 m above the ground in Park Falls and 31, 99, and 379 m above the ground in West Branch. Observations were made several times over 10-min periods

Validation of GOSAT XCO₂ using aircraft measurement

M. Inoue et al.

Title Page

Abstract

Introduction

Conclusions

References

Tables

Figures

◀

▶

◀

▶

Back

Close

Full Screen / Esc

Printer-friendly Version

Interactive Discussion



and every 30 s for the highest altitudes. We used averages of the data obtained within ± 10 min of the sampling time by the aircraft at each altitude to calculate XCO_2 .

3 Analysis methods

3.1 XCO_2 calculation from aircraft data

3.1.1 Tropospheric profiles and the tropopause height

The XCO_2 calculation method from aircraft data in this study was equivalent to that described previously by Miyamoto et al. (2012). Due to the limited range of altitudes for aircraft measurements, further observational data or certain assumptions were required near the surface and in the middle atmosphere. Araki et al. (2010) determined that the uncertainty of XCO_2 over Tsukuba calculated using aircraft data at one aircraft measurement site of Narita was estimated to be ~ 1 ppm and calculating XCO_2 from airliners could be applied to the validation of GOSAT products. CO_2 profiles in the troposphere were constructed in a manner similar to that described by Araki et al. (2010). Where tower data were available, they were used near the surface to complement the CO_2 profiles of aircraft-based data. Where there were no tower data for a site, we extrapolated profiles obtained by the aircraft to the surface from the lowest measured aircraft data. When an airliner did not fly above the tropopause, the CO_2 concentration at the highest observational altitude was assumed to be constant up to the tropopause. The local tropopause height was determined from the Global Forecast System (GFS) model (<http://nomads.ncdc.noaa.gov/>) produced by the National Centers for Environmental Prediction (NCEP), and was in good agreement with radiosonde measurements (Pan and Munchak, 2011). In this study, we used the GFS tropopause height data provided as reanalysis values at 00:00, 06:00, 12:00, and 18:00 UTC and the forecast values at 03:00, 09:00, 12:00, and 21:00 UTC (3 h after the reanalysis time) with $1^\circ \times 1^\circ$ horizontal grids. For aircraft profiles that were measured higher than the local

Validation of GOSAT XCO_2 using aircraft measurement

M. Inoue et al.

Title Page

Abstract

Introduction

Conclusions

References

Tables

Figures

◀

▶

◀

▶

Back

Close

Full Screen / Esc

Printer-friendly Version

Interactive Discussion



tropopause, model outputs in the stratosphere (see Sect. 3.1.2) were added above the highest aircraft measurement.

3.1.2 Profiles of the stratosphere and mesosphere

To complete stratospheric and mesospheric profiles, Araki et al. (2010) used an empirical model of profiles at mid-latitudes in the Northern Hemisphere. We used profiles derived from the mean “age of air”, defined as the time required for an air parcel to transit from the Earth’s surface to the layers above (Kida, 1983), at various altitudes according to the method described by Miyamoto et al. (2012) in order to apply the method of Araki et al. (2010) to the XCO₂ calculation at various regions. The “age of air” was determined from the Center for Climate System Research/National Institute for Environmental Studies/Frontier Research Center for Global Change (CCSR/NIES/FRCGC) atmospheric general circulation model (AGCM; Numaguti et al., 1997)-based chemical transport model (referred to as the ACTM; Patra et al., 2009). The age was converted to a CO₂ mixing ratio by assuming a tropospheric concentration (corresponding to a 0-yr-old mixing ratio) in 2006 of 381.2 ppm and an annual trend of 1.9 ppm yr⁻¹ at every site (WMO, 2007). The actual global mean CO₂ concentration in 2009 was 386.8 ppm (WMO, 2010), and the actual mean annual trend during 2006–2009 was approximately 1.9 ppm yr⁻¹. The vertical structure of the CO₂ concentration estimated by the age of air was consistent with balloon measurements of CO₂ over Japan (Nakazawa et al., 1995; Miyamoto et al., 2012). Although ACTM was used for profiles of the stratosphere and mesosphere in this study, we evaluated the impact of profiles in the middle atmosphere on the aircraft-based XCO₂ calculation using the two other model outputs discussed in Sect. 4.2.

3.1.3 Dry air number density profiles

To obtain the number density profiles of dry air, we utilized meteorological data from the Committee on Space Research (COSPAR) International Reference Atmosphere

Validation of GOSAT XCO₂ using aircraft measurement

M. Inoue et al.

Title Page

Abstract

Introduction

Conclusions

References

Tables

Figures



Back

Close

Full Screen / Esc

Printer-friendly Version

Interactive Discussion



Validation of GOSAT XCO₂ using aircraft measurement

M. Inoue et al.

Title Page

Abstract

Introduction

Conclusions

References

Tables

Figures

◀

▶

◀

▶

Back

Close

Full Screen / Esc

Printer-friendly Version

Interactive Discussion



(CIRA-86; Fleming et al., 1990), which provides empirical models of atmospheric temperature and air number densities from the surface to 120 km. We estimated the aircraft-based XCO₂ using the air number densities of CIRA-86 and grid point value (GPV) data from a numerical weather prediction model developed by the Japan Meteorological Agency (e.g. Nakakita et al., 1996). The aircraft-based XCO₂ data where air number densities of GPV were used below 10 hPa and CIRA-86 above 10 hPa (GPV-CIRA XCO₂) were compared to values calculated using the CIRA-86 data vertically throughout the atmosphere (CIRA XCO₂). We estimated an average of 113 cases obtained at the Narita site in 2009. The results showed that an average and ± 1 standard deviation (1σ) of the differences between “CIRA XCO₂” and “GPV-CIRA XCO₂” were as small as 0.0005 ± 0.0326 ppm. In addition, Araki et al. (2010) also indicated that the XCO₂ calculated by air number densities of CIRA-86 was in agreement with values calculated from a rawinsonde over Tsukuba to within 0.08 ppm. Therefore, we used the air number densities obtained solely by CIRA-86 as the air number densities of dry air in this study.

3.1.4 Aircraft-based CO₂ profiles and XCO₂ with and without column averaging kernel (CAK)

An example of aircraft-based CO₂ profiles is shown in Fig. 2. The open circles and triangles represent aircraft measurement data and tower data, respectively. In addition, the solid and dashed lines show the observed (i.e. based on in situ measurements) and assumed CO₂ profiles, respectively. Based on aircraft-based CO₂ profiles, XCO₂ with and without applying CAK is calculated.

CAK \mathbf{a} is defined as

$$\mathbf{a}_j = (\mathbf{h}^T \mathbf{A})_j \frac{1}{h_j} \quad (1)$$

where the subscript j denotes the index of the j -th layer, \mathbf{A} is the averaging kernel matrix, and \mathbf{h} is a pressure weighting function calculated based on the dry air number

density profile (Connor et al., 2008; Ohyama et al., 2009; Yoshida et al., 2010). CAK is a function of pressure and solar zenith angle. The X_{CO_2} values for the aircraft profile that is weighted by the CO_2 CAK \mathbf{a} are calculated according to the method of Rodgers and Connor (2003) and Connor et al. (2008).

$$\begin{aligned}
 X_{CO_2}^{\text{in-situ, CAK}} &= X_{CO_2}^a + \sum_j h_j \mathbf{a}_j (\mathbf{t}_{\text{in-situ}} - \mathbf{t}_a)_j \\
 &= \mathbf{h}^T [\mathbf{A} \cdot \mathbf{t}_{\text{in-situ}} + (\mathbf{I} - \mathbf{A}) \mathbf{t}_a]
 \end{aligned}
 \tag{2}$$

where $X_{CO_2}^a$ is the column-averaged volume mixing ratio of CO_2 for the a priori profile \mathbf{t}_a , and $\mathbf{t}_{\text{in-situ}}$ is the aircraft-based CO_2 profile. The a priori CO_2 profile for GOSAT is calculated for every observation day by an offline global atmospheric transport model developed by NIES (NIES TM; Maksyutov et al., 2008). GOSAT a priori profiles make some effects on X_{CO_2} retrieval. On the other hand, aircraft-based X_{CO_2} without applying the CO_2 CAK can be expressed as

$$X_{CO_2}^{\text{in-situ, noCAK}} = \mathbf{h}^T \cdot \mathbf{t}_{\text{in-situ}}
 \tag{3}$$

Note that the actual altitudinal integration of Eq. (3) was conducted from the ground up to the altitude of the mesopause (~ 85 km) with a vertical resolution of 100 m based on the method described by Araki et al. (2010). Miyamoto et al. (2012) defined and estimated the uncertainty of the X_{CO_2} calculation from the aircraft profile for each flight based on four domains. In this study, we made GOSAT X_{CO_2} validation using the aircraft-based X_{CO_2} data with an uncertainty of less than 1 ppm.

When comparing of GOSAT SWIR X_{CO_2} with the gap-filling time series of the aircraft-based X_{CO_2} through curve fitting (see Sect. 3.2), GOSAT SWIR CAK cannot be applied due to the absence of the vertical information for all aircraft measurements. Therefore, we first evaluated the impact of GOSAT SWIR CAK on the aircraft-based X_{CO_2} calculation (Sect. 4.1).

**Validation of GOSAT
 X_{CO_2} using aircraft
measurement**

M. Inoue et al.

Title Page

Abstract

Introduction

Conclusions

References

Tables

Figures

◀

▶

◀

▶

Back

Close

Full Screen / Esc

Printer-friendly Version

Interactive Discussion



3.2 Validation method for GOSAT products using aircraft data

Based on the results of the impacts of GOSAT SWIR CAK on the XCO₂ calculation, we performed a comparison of the GOSAT data retrieved within $\pm 2^\circ$ or $\pm 5^\circ$ latitude/longitude boxes centered at each observation site and aircraft-based data measured on a GOSAT overpass day (i.e. extraction of temporally matched cases with direct comparison). The aircraft data temporally nearest the GOSAT overpass time were selected where there were multiple aircraft data associated with the particular GOSAT data. Scatter diagrams between GOSAT XCO₂ and aircraft-based XCO₂ are presented for land and ocean separately, and correlation coefficients and their differences are estimated as described in Sect. 4.3.1.

This extraction method enabled us to validate GOSAT products using the temporally matched observational data. However, this method resulted in no temporally matched data at some observation sites where no aircraft measurements were made on the GOSAT overpass day. Therefore, we prepared temporally interpolated aircraft-based XCO₂ data by fitting a curve containing annual trends and annual/semiannual sinusoidal variations to compare with GOSAT XCO₂. Examples for several aircraft observation sites and scatter diagrams for all sites are presented in Sect. 4.3.2 and the results for each site are shown in the Supplement.

4 Results

4.1 Impact of GOSAT SWIR CAK on the aircraft-based XCO₂ calculation

The impact of the GOSAT SWIR CAK on the aircraft-based XCO₂ calculation was evaluated for each observation site. We made a connection between aircraft-based data at certain time of the day and the GOSAT data nearest to the aircraft observation site for all GOSAT data obtained within $\pm 10^\circ$ latitude/longitude boxes centered at the observation site on the same day. In this study, XCO₂ calculated from the aircraft-based data

ACPD

13, 3203–3246, 2013

Validation of GOSAT XCO₂ using aircraft measurement

M. Inoue et al.

Title Page

Abstract

Introduction

Conclusions

References

Tables

Figures

◀

▶

◀

▶

Back

Close

Full Screen / Esc

Printer-friendly Version

Interactive Discussion



weighted with a selected GOSAT SWIR CAK using Eq. (2) was expressed as “aircraft-based XCO_2 with CAK”, whereas XCO_2 calculated from the aircraft-based data without the application of GOSAT CAK using Eq. (3) was expressed as “aircraft-based XCO_2 without CAK”.

Before evaluation of the GOSAT CAK impacts, we consider examples of vertical profiles of CO_2 density and CAK over several locations. In Fig. 3, black lines, blue open circles, and triangles indicate the GOSAT SWIR CAK and profiles of the aircraft and tower measurements of CO_2 over Narita, respectively. Red lines indicate the GOSAT a priori profiles of CO_2 , which were calculated for the day of observation by NIES TM. The atmosphere was divided into 15 layers from the surface to 0.1 hPa with a constant pressure difference. We focused on 28 June 2009 (Fig. 3a), when the difference between aircraft-based XCO_2 with and without the application of CAK was larger (0.132 ppm) over Narita during the analysis period. As is clear from Fig. 3a, the XCO_2 values of tower measurement were not coincident with those of GOSAT a priori. It was assumed that this disagreement (i.e. the shape of the a priori profile) was one reason for the increase in XCO_2 difference associated with the application of CAK. Figure 3e shows the vertical structures of GOSAT CAK and CO_2 density on 19 March 2010. CAK was around 1 from about 3 to 5 km and decreased monotonically with height. Aircraft data (about 1.3–11 km) and the tower data (1.5–200 m) demonstrated that the CO_2 concentration was higher in the lower troposphere and lower in the middle and upper troposphere, which was similar to the GOSAT a priori profile. Above the highest observational point of the airliner, an assumed line including ACTM was similar in structure to the a priori profile. Under these conditions, the difference between XCO_2 with CAK and XCO_2 without CAK was as small as -0.033 ppm. In the case of 6 April 2010, vertical profiles of the aircraft and tower agreed well with those of the a priori profile (Fig. 3f), and hence the difference between aircraft-based XCO_2 with and without CAK was as small as 0.046 ppm.

Next, we present some examples from observation sites other than Narita. Figure 4a and b shows examples of vertical profiles in Honolulu, Hawaii. As there is

Validation of GOSAT XCO_2 using aircraft measurement

M. Inoue et al.

Title Page

Abstract

Introduction

Conclusions

References

Tables

Figures

◀

▶

◀

▶

Back

Close

Full Screen / Esc

Printer-friendly Version

Interactive Discussion



Validation of GOSAT XCO₂ using aircraft measurement

M. Inoue et al.

Title Page

Abstract

Introduction

Conclusions

References

Tables

Figures

◀

▶

◀

▶

Back

Close

Full Screen / Esc

Printer-friendly Version

Interactive Discussion

no meteorological tower, the concentration of the lowest observational altitude of an airliner has been extended down to the surface. On 18 August 2009, the CO₂ concentration was lower in the upper troposphere and higher above the tropopause (Fig. 4b). This may be explained by meridional transport of CO₂ from the tropical troposphere in the Northern summer (Sawa et al., 2008). An example for Sydney (Australia) is shown in Fig. 4c. As shown below, the seasonal variation of CO₂ over the Southern Hemisphere (Fig. 5b) is not clearer than that over the Northern Hemisphere (e.g. Fig. 5a). On 22 March 2010, the CO₂ density recorded by aircraft measurements was constant from about 3 to 12 km (Fig. 4c) and the XCO₂ difference associated with CAK was −0.089 ppm. In the Southern Great Plains (Oklahoma, USA), two examples for the Northern summer and winter are given (Fig. 4d, e). The CO₂ concentration is clearly lower near the surface and higher in the mid-troposphere in summer, whereas CO₂ densities in winter decrease with height. We also show an example in Park Falls using NOAA tower data in Fig. 4f.

Figure 5a shows the temporal variations of aircraft-based XCO₂ over Narita (Northern Hemisphere) from June 2009 to July 2010. A total of 225 temporally matched cases were obtained. Both data with and without CAK showed that XCO₂ is higher in spring and lower from late summer through autumn. Open triangles denote the differences, which are less than ±0.2 ppm in most cases. As listed in Table 2, the average of all differences in Narita is as small as -0.030 ± 0.095 ppm, and it can be assumed that the GOSAT SWIR CAK has only a minor effect on the aircraft-based XCO₂ calculation over Narita. We also present temporal variations and the impacts of GOSAT CAK for Sydney, the Southern Great Plains, Bangkok (Thailand), Honolulu, and Briggsdale (Colorado, USA) (Fig. 5b–f). The Southern Great Plains had the second highest number of samples among 17 NOAA sites (Table 2). Temporally matched data were confined to the period between late spring and early autumn in Honolulu (Fig. 5e). This may be attributed to sunglint observation which is conducted by utilizing specular reflection over certain ocean regions where surface reflectance is small (e.g. Kuze et al., 2009).

Consequently, 663 samples were extracted from 41 observation sites and the average of all differences was -0.021 ± 0.089 ppm (Table 2).

The differences between aircraft-based XCO_2 with CAK and without CAK were evaluated to be less than ± 0.4 ppm at most, and less than -0.1 ppm on average (Table 2). Therefore, we concluded that the GOSAT SWIR CAK had a minor effect on the aircraft-based XCO_2 calculation. The GOSAT validation using aircraft-based XCO_2 with GOSAT CAK is presented in Sect. 4.3.1.

4.2 Impact of model profiles in the stratosphere and mesosphere on the aircraft-based XCO_2 calculation

In addition to ACTM, two more model outputs were used as the middle atmosphere profiles to investigate the impact. We calculated XCO_2 from aircraft profiles using ACTM, a priori profiles as in GOSAT retrieval (Maksyutov et al., 2008, see Sect. 3.1.4), and a priori profiles of TCCON (Wunch et al., 2010) as stratospheric and mesospheric profiles at four aircraft sites (Park Falls, the Southern Great Plains, Narita, and Sydney), located near the TCCON sites – Park Falls, Lamont (Oklahoma, USA), Tsukuba (Japan), and Wollongong (Australia). Column abundances calculated from the three model profiles were referred to as “ACTM XCO_2 ”, “GOSAT prior XCO_2 ”, and “TCCON prior XCO_2 ”, respectively. Figure 6 shows an example for Narita on 28 November 2009, including profiles by ACTM, GOSAT a priori profile, and TCCON a priori profile. Here, the difference between “ACTM XCO_2 ” and “GOSAT prior XCO_2 ” was as small as 0.011 ppm and the difference between “ACTM XCO_2 ” and “TCCON prior XCO_2 ” was -0.133 ppm. The averages obtained at the four respective observation sites are listed in Table 3. The average of “ACTM XCO_2 minus TCCON prior XCO_2 ” over Park Falls was -0.311 ± 0.076 ppm. This result was consistent with that of Saito et al. (2012) who showed that the XCO_2 difference between the ACTM and TCCON was -0.4 ppm (note that their results were based on profiles in all layers of the ACTM and TCCON). The results of 116 examples obtained at four observation sites indicated that the difference between “ACTM XCO_2 ” and “GOSAT prior XCO_2 ” was as small as

Validation of GOSAT XCO_2 using aircraft measurement

M. Inoue et al.

Title Page

Abstract

Introduction

Conclusions

References

Tables

Figures

◀

▶

◀

▶

Back

Close

Full Screen / Esc

Printer-friendly Version

Interactive Discussion



0.125 ± 0.334 ppm. On the other hand, “ACTM XCO₂ minus TCCON prior XCO₂” was -0.161 ± 0.098 ppm. Although the XCO₂ differences varied by region, the amount of CO₂ above the tropopause was small and consequently did not have a large effect on the aircraft-based XCO₂ calculation at the four observation sites.

4.3 Comparison between GOSAT XCO₂ and aircraft-based XCO₂

4.3.1 Comparison analysis by temporally matched cases

We compared the GOSAT data observed within ±2° and ±5° latitude/longitude boxes centered at each observation site. Figure 7 shows comparisons between aircraft-based XCO₂ with the application of CAK and GOSAT data. In addition, the average and 1σ of the differences between GOSAT XCO₂ and aircraft-based XCO₂ at each site and for all sites are listed in Table 4. For the ±2° boxes, there were a total of 71 observations over land and 9 over oceans, whereas there were a total of 177 observations over land and 37 over oceans for the ±5° boxes. In ocean regions, GOSAT data were underestimated by 1.64 ± 1.05 ppm and 2.29 ± 1.84 ppm for the ±2° and ±5° boxes, respectively, compared to reference data. Correlation coefficients between both data sets were 0.97 and 0.82 with significance at the 99% level, for XCO₂ data within the ±2° and ±5° boxes, respectively. Over the land regions, GOSAT SWIR XCO₂ had a low bias of 0.75 ± 2.57 ppm and 1.01 ± 2.51 ppm and the correlation coefficients were 0.85 and 0.86 with significance at the 99% level for the ±2° and ±5° boxes, respectively. The negative bias of XCO₂ retrieved in the ocean region was larger than that for the land region. This difference may be attributed to the fact that the reflectances of the land and ocean surfaces are represented by the surface albedo and the surface wind speed, respectively (Yoshida et al., 2011). However, the variance over land was about 1 ppm larger than that over ocean regions. Aerosols and clouds are major sources of disturbance in GHG observations from space due to modification of the equivalent optical path length (Mao and Kawa, 2004; Houweling et al., 2005; Reuter et al., 2010) and have a significant impact on the retrieval of GOSAT SWIR XCO₂ (Uchino et al., 2012).

Validation of GOSAT XCO₂ using aircraft measurement

M. Inoue et al.

Title Page

Abstract

Introduction

Conclusions

References

Tables

Figures

◀

▶

◀

▶

Back

Close

Full Screen / Esc

Printer-friendly Version

Interactive Discussion



The atmosphere over ocean regions appears to be cleaner due to the absence of polluted air and aerosols from urban areas, whereas GOSAT XCO₂ retrieval in several land regions may be profoundly affected by polluted air and urban aerosols.

Our results suggest that the present version (Ver. 02.00) of GOSAT FTS-SWIR XCO₂ products is a significant improvement on the previous version (Ver. 01.xx), which produced values approximately 9 ppm lower than ground-based FTS data in several locations across the globe (Morino et al., 2011). In addition, the present version (Ver. 02.00) of GOSAT XCO₂ observed over both land and ocean regions agreed with aircraft measurement data.

4.3.2 Comparison by curve fitting method

As noted in Sect. 3.2, it was difficult to compare GOSAT products with aircraft measurement data at some observation sites (about one third of the total sites used for temporally matched cases in the present study) where there was a paucity of flight data on the day when GOSAT was scheduled to overpass. The temporal interpolation of aircraft-based XCO₂ by a curve fitting method enabled temporally matched cases to be obtained for all observation sites. Curve fitting methods were used to detect or quantify the upward trends, the presence of seasonal cycles, and short-term fluctuations that are notable features of a CO₂ time series (e.g. Nakazawa et al., 1997a). We attempted to fit aircraft-based XCO₂ using the same method as used by Miyamoto et al. (2012) with Eq. (4) containing annual trend and annual/semiannual sinusoidal variations.

$$\text{XCO}_2(t) = \text{Intercept} + \text{Trend} \times t + \frac{\text{Amp}_1}{2} \times \cos\left(2\pi \frac{t - \phi_1}{12}\right) + \frac{\text{Amp}_2}{2} \times \cos\left(4\pi \frac{t - \phi_2}{12}\right) \quad (4)$$

where XCO₂(*t*) is the XCO₂ value at time *t*, Intercept denotes the column abundance on 1 January 2007 without sinusoidal variations, and Trend represents the monthly growth rate, Amp₁ and Amp₂ are sinusoidal variations with periods of one year and a half year, respectively, and φ₁ and φ₂ are phases in the annual and semiannual

Validation of GOSAT XCO₂ using aircraft measurement

M. Inoue et al.

Title Page

Abstract

Introduction

Conclusions

References

Tables

Figures

◀

▶

◀

▶

Back

Close

Full Screen / Esc

Printer-friendly Version

Interactive Discussion



Validation of GOSAT XCO₂ using aircraft measurement

M. Inoue et al.

Title Page

Abstract

Introduction

Conclusions

References

Tables

Figures

◀

▶

◀

▶

Back

Close

Full Screen / Esc

Printer-friendly Version

Interactive Discussion



sinusoidal variations, respectively. Miyamoto et al. (2012) provided more information regarding use of the equation. We converted aircraft-based XCO₂ without CAK after 2007 into an XCO₂ time series (i.e. continuous data) by curve fitting. The GOSAT XCO₂ data observed within the $\pm 2^\circ$ and $\pm 5^\circ$ latitude/longitude boxes centered at each aircraft measurement site were compared with the fitted values based on the aircraft-based XCO₂. The results of the comparison for the $\pm 5^\circ$ boxes centered at several sites are shown in Fig. 8. For many observation sites at mid- and high-latitudes over the Northern Hemisphere – i.e. Amsterdam (The Netherlands), Narita, North America, and Siberia – aircraft-based XCO₂ displayed a seasonal amplitude of approximately 7–8 ppm. The growth rate of aircraft-based XCO₂ was about 2 ppm yr⁻¹ at most sites, which corresponded to previous studies of CO₂ variations (e.g. Washenfelder et al., 2006; Yang et al., 2007; Ohyama et al., 2009). At Narita, the average of the differences between GOSAT XCO₂ over land region within $\pm 5^\circ$ of the site and aircraft-based XCO₂ was considerably small at -0.55 ± 2.47 ppm, whereas the value in the Southern Great Plains was -2.75 ± 1.93 ppm. The correlation coefficients between both data sets were 0.65–0.85 over land and 0.61–0.92 over oceans for many regions, including Asia, North America, Europe, and Siberia. The detailed comparisons (temporal variations and scatter diagrams) for each observation site using the curve fitting method are shown in the Supplementary materials.

Figure 9 shows the scatter diagrams between GOSAT SWIR XCO₂ and aircraft-based XCO₂ (estimated values at the GOSAT overpass time) obtained by the curve fitting method at all observation sites. In ocean regions, GOSAT data were underestimated by about 1.52 ± 2.02 ppm and 1.73 ± 2.35 ppm compared to reference data for the $\pm 2^\circ$ and $\pm 5^\circ$ boxes, respectively (Table 5). GOSAT SWIR XCO₂ over the land regions had a low bias of 1.56 ± 2.36 ppm and 1.81 ± 2.37 ppm for the $\pm 2^\circ$ and $\pm 5^\circ$ boxes, respectively. The biases for land regions estimated by curve fitting seemed to be larger than those recorded by comparison of temporally matched cases. However, we found prominent positive correlations between GOSAT XCO₂ and aircraft-based XCO₂ for both land and ocean regions. In land regions, the correlation coefficients were 0.81

with significance at the 99 % level for both $\pm 2^\circ$ and $\pm 5^\circ$ boxes. Over ocean regions, the correlation coefficients were 0.72 and 0.75 with significance at the 99 % level, respectively, for $\pm 2^\circ$ and $\pm 5^\circ$ boxes. GOSAT data were biased by about 1–2 ppm. These results were consistent with those of the direct comparison by temporally matched cases described in Sect. 4.3.1 (Fig. 7).

5 Summary and conclusions

This paper presents a validation of XCO₂ derived from GOSAT TANSO-FTS SWIR (Ver. 02.00) using aircraft measurement data obtained from CONTRAIL, NOAA, and NIES. Prior to the GOSAT validation, we examined how the aircraft-based XCO₂ changes following application of the GOSAT SWIR CAK. The differences between aircraft-based XCO₂ with and without CAK were evaluated to be less than ± 0.4 ppm at most, and less than 0.1 ppm on average. Therefore, we concluded that the GOSAT CAK had only a minor effect on the aircraft-based XCO₂ calculation.

We performed a comparison between GOSAT SWIR XCO₂ observed within $\pm 2^\circ$ or $\pm 5^\circ$ latitude/longitude boxes at each site and aircraft-based XCO₂ measured on a GOSAT overpass day. The results indicated that GOSAT XCO₂ data agreed well with aircraft measurement data except for negative biases of 1–2 ppm (with a standard deviation of 1–3 ppm) in the GOSAT data. The present version (Ver. 02.00) of GOSAT SWIR products was a significant improvement on the earlier version (Ver. 01.xx), which produced values approximately 9 ppm lower than reference data. However, the standard deviations of the differences between GOSAT XCO₂ and aircraft-based XCO₂ were not as small being around 3 ppm at several sites. Further studies are required to investigate the causes of this finding with a focus on the correlation between GOSAT SWIR XCO₂ and several simultaneously retrieved variables, including aerosol optical depth and surface albedo.

Validation of GOSAT XCO₂ using aircraft measurement

M. Inoue et al.

Title Page

Abstract

Introduction

Conclusions

References

Tables

Figures

◀

▶

◀

▶

Back

Close

Full Screen / Esc

Printer-friendly Version

Interactive Discussion



Supplementary material related to this article is available online at:
[http://www.atmos-chem-phys-discuss.net/13/3203/2013/
acpd-13-3203-2013-supplement.pdf](http://www.atmos-chem-phys-discuss.net/13/3203/2013/acpd-13-3203-2013-supplement.pdf).

Acknowledgements. The authors thank the many staff members of Japan Airlines, the JAL Foundation, and JAMCO Tokyo for supporting the CONTRAIL project. We are grateful to the NOAA ESRL/GMD tall tower network (K. Davis, A. Desai, R. Teclaw, D. Baumann, and C. Stanier) for providing LEF and WBI CO₂ tower data. This research was supported in part by the Environment Research and Technology Development Fund (A-1102) of the Ministry of the Environment, Japan.

References

Andrews, A. E., Kofler, J., Bakwin, P. S., Zhao, C., and Tans, P.: Carbon dioxide and carbon monoxide dry air mole fractions from the NOAA ESRL tall tower network, 1992–2009, Version: 2011-08-31, available at: <ftp://ftp.cmdl.noaa.gov/ccg/towers/> (last access: January 2013), 2011.

Araki, M., Morino, I., Machida, T., Sawa, Y., Matsueda, H., Ohyama, H., Yokota, T., and Uchino, O.: CO₂ column-averaged volume mixing ratio derived over Tsukuba from measurements by commercial airlines, *Atmos. Chem. Phys.*, 10, 7659–7667, doi:10.5194/acp-10-7659-2010, 2010.

Buchwitz, M., de Beek, R., Burrows, J. P., Bovensmann, H., Warneke, T., Notholt, J., Meirink, J. F., Goede, A. P. H., Bergamaschi, P., Körner, S., Heimann, M., and Schulz, A.: Atmospheric methane and carbon dioxide from SCIAMACHY satellite data: initial comparison with chemistry and transport models, *Atmos. Chem. Phys.*, 5, 941–962, doi:10.5194/acp-5-941-2005, 2005.

Chédin, A., Serrar, S., Armante, R., and Scott, N. A.: Signatures of annual and seasonal variations of CO₂ and other greenhouse gases from comparisons between NOAA TOVS observations and radiation model simulations, *J. Climate*, 15, 95–116, 2002.

ACPD

13, 3203–3246, 2013

Validation of GOSAT XCO₂ using aircraft measurement

M. Inoue et al.

Title Page

Abstract

Introduction

Conclusions

References

Tables

Figures

◀

▶

◀

▶

Back

Close

Full Screen / Esc

Printer-friendly Version

Interactive Discussion



**Validation of GOSAT
XCO₂ using aircraft
measurement**

M. Inoue et al.

Title Page

Abstract

Introduction

Conclusions

References

Tables

Figures

◀

▶

◀

▶

Back

Close

Full Screen / Esc

Printer-friendly Version

Interactive Discussion

Christi, M. J. and Stephens, G. L.: Retrieving profiles of atmospheric CO₂ in clear sky and in the presence of thin cloud using spectroscopy from the near and thermal infrared: a preliminary case study, *J. Geophys. Res.*, 109, D04316, doi:10.1029/2003JD004058, 2004.

Connor, B. J., Bösch, H., Toon, G., Sen, B., Miller, C., and Crisp, D.: Orbiting carbon observatory: inverse method and prospective error analysis, *J. Geophys. Res.*, 113, D05305, doi:10.1029/2006JD008336, 2008.

Conway, T. J., Tans, P., Waterman, L. S., Thoning, K. W., Masarie, K. A., and Gammon, R. H.: Atmospheric carbon dioxide measurements in the remote global troposphere, 1981–1984, *Tellus B*, 40, 81–115, 1988.

Crevoisier, C., Heilliette, S., Chédin, A., Serrar, S., Armante, R., and Scott, N. A.: Midtropospheric CO₂ concentration retrieval from AIRS observations in the tropics, *Geophys. Res. Lett.*, 31, L17106, doi:10.1029/2004GL020141, 2004.

Dils, B., De Mazière, M., Müller, J. F., Blumenstock, T., Buchwitz, M., de Beek, R., Demoulin, P., Duchatelet, P., Fast, H., Frankenberg, C., Gloudemans, A., Griffith, D., Jones, N., Kerzenmacher, T., Kramer, I., Mahieu, E., Mellqvist, J., Mittermeier, R. L., Notholt, J., Rinsland, C. P., Schrijver, H., Smale, D., Strandberg, A., Straume, A. G., Stremme, W., Strong, K., Sussmann, R., Taylor, J., van den Broek, M., Velazco, V., Wagner, T., Warneke, T., Wiacek, A., and Wood, S.: Comparisons between SCIAMACHY and ground-based FTIR data for total columns of CO, CH₄, CO₂ and N₂O, *Atmos. Chem. Phys.*, 6, 1953–1976, doi:10.5194/acp-6-1953-2006, 2006.

Enting, I. G.: *Inverse problems in atmospheric constituent transport*, Cambridge University Press, Cambridge, UK, 393 pp., 2002.

Fleming, E. L., Chandra, S., Barnett, J. J., and Corney, M.: Zonal mean temperature, pressure, zonal wind and geopotential height as functions of latitude, COSPAR international reference atmosphere: 1986, part II: middle atmosphere models, *Adv. Space Res.*, 10, 11–59, doi:10.1016/0273-1177(90)90386-E, 1990.

Gurney, K. R., Law, R. M., Denning, A. S., Rayner, P. J., Baker, D., Bousquet, P., Bruhwiler, L., Chen, Y.-H., Ciais, P., Fan, S., Fung, I. Y., Gloor, M., Heimann, M., Higuchi, K., John, J., Maki, T., Maksyutov, S., Masarie, K., Peylin, P., Prather, M., Pak, B. C., Randerson, J., Sarmiento, J., Taguchi, S., Takahashi, T., and Yuen, C.-W.: Towards robust regional estimates of CO₂ sources and sinks using atmospheric transport models, *Nature*, 415, 626–630, doi:10.1038/415626a, 2002.

Validation of GOSAT XCO₂ using aircraft measurement

M. Inoue et al.

Title Page

Abstract

Introduction

Conclusions

References

Tables

Figures

◀

▶

◀

▶

Back

Close

Full Screen / Esc

Printer-friendly Version

Interactive Discussion



Heymann, J., Bovensmann, H., Buchwitz, M., Burrows, J. P., Deutscher, N. M., Notholt, J., Rettinger, M., Reuter, M., Schneising, O., Sussmann, R., and Warneke, T.: SCIAMACHY WFM-DOAS XCO₂: reduction of scattering related errors, *Atmos. Meas. Tech.*, 5, 2375–2390, doi:10.5194/amt-5-2375-2012, 2012.

5 Houweling, S., Hartmann, W., Aben, I., Schrijver, H., Skidmore, J., Roelofs, G.-J., and Breon, F.-M.: Evidence of systematic errors in SCIAMACHY-observed CO₂ due to aerosols, *Atmos. Chem. Phys.*, 5, 3003–3013, doi:10.5194/acp-5-3003-2005, 2005.

Inoue, H. Y. and Matsueda, H.: Variations in atmospheric CO₂ at the Meteorological Research Institute, Tsukuba, Japan, *J. Atmos. Chem.*, 23, 137–161, 1996.

10 Inoue, H. Y. and Matsueda, H.: Measurements of atmospheric CO₂ from a meteorological tower in Tsukuba, Japan, *Tellus B*, 53, 205–219, doi:10.1034/j.1600-0889.2001.01163.x, 2001.

Kida, H.: General circulation of air parcels and transport characteristics derived from a hemispheric GCM, part 2, very long-term motions of air parcels in the troposphere and stratosphere, *J. Meteor. Soc. Jpn.*, 61, 510–522, 1983.

15 Komhyr, W. D., Harris, T. B., Waterman, L. S., Chin, J. F. S., and Thoning, K. W.: Atmospheric carbon dioxide at Mauna Loa Observatory 1. NOAA global monitoring for climatic change measurements with a nondispersive infrared analyzer, 1974–1985, *J. Geophys. Res.*, 94, 8533–8547, doi:10.1029/JD094iD06p08533, 1989.

20 Kuze, A., Suto, H., Nakajima, M., and Hamazaki, T.: Thermal and near infrared sensor for carbon observation Fourier-transform spectrometer on the Greenhouse Gases Observing Satellite for greenhouse gases monitoring, *Appl. Optics*, 48, 6716–6733, doi:10.1364/AO.48.006716, 2009.

Machida, T., Nakazawa, T., Ishidoya, S., Maksyutov, S., Tohjima, Y., Takahashi, Y., Watai, T., Vinnichenko, N., Panchenko, M., Arshinov, M., Fedoseev, N., and Inoue, G.: Temporal and spatial variations of atmospheric CO₂ mixing ratio over Siberia, *Ext. Abstr.*, in: 6th International CO₂ Conf., 1–5 October, Sendai, Japan, 2001.

25 Machida, T., Matsueda, H., Sawa, Y., Nakagawa, Y., Hirotani, K., Kondo, N., Goto, K., Nakazawa, T., Ishikawa, K., and Ogawa, T.: Worldwide measurements of atmospheric CO₂ and other trace gas species using commercial airlines, *J. Atmos. Oceanic. Tech.*, 25, 1744–1754, doi:10.1175/2008JTECHA1082.1, 2008.

30 Maddy, E. S., Barnet, C. D., Goldberg, M., Sweeney, C., and Liu, X.: CO₂ retrievals from the atmospheric infrared sounder: methodology and validation, *J. Geophys. Res.*, 113, D11301, doi:10.1029/2007JD009402, 2008.

**Validation of GOSAT
XCO₂ using aircraft
measurement**

M. Inoue et al.

Title Page

Abstract

Introduction

Conclusions

References

Tables

Figures

◀

▶

◀

▶

Back

Close

Full Screen / Esc

Printer-friendly Version

Interactive Discussion



Maksyutov, S., Patra, P. K., Onishi, R., Saeki, T., and Nakazawa, T.: NIES/FRCGC global atmospheric tracer transport model: description, validation, and surface sources and sinks inversion, *J. Earth Sim.*, 9, 3–18, 2008.

Mao, J. and Kawa, S. R.: Sensitivity studies for space-based measurement of atmospheric total column carbon dioxide by reflected sunlight, *Appl. Optics*, 43, 914–927, 2004.

Matsueda, H., Inoue, H. Y., and Ishii, M.: Aircraft observation of carbon dioxide at 8–13 km altitude over the Western Pacific from 1993 to 1999, *Tellus B*, 54, 1–21, 2002.

Matsueda, H., Machida, T., Sawa, Y., Nakagawa, Y., Hirokani, K., Ikeda, H., Kondo, N., and Goto, K.: Evaluation of atmospheric CO₂ measurements from new flask air sampling of JAL airliner observations, *Pap. Meteorol. Geophys.*, 59, 1–17, 2008.

Miyamoto, Y., Inoue, M., Morino, I., Uchino, O., Yokota, T., Machida, T., Sawa, Y., Matsueda, H., Sweeney, C., Tans, P. P., Andrews, A. E., and Patra, P. K.: Atmospheric column-averaged mole fractions of carbon dioxide at 53 aircraft measurement sites, *Atmos. Chem. Phys. Discuss.*, 12, 28493–28523, doi:10.5194/acpd-12-28493-2012, 2012.

Morino, I., Uchino, O., Inoue, M., Yoshida, Y., Yokota, T., Wennberg, P. O., Toon, G. C., Wunch, D., Roehl, C. M., Notholt, J., Warneke, T., Messerschmidt, J., Griffith, D. W. T., Deutscher, N. M., Sherlock, V., Connor, B., Robinson, J., Sussmann, R., and Rettinger, M.: Preliminary validation of column-averaged volume mixing ratios of carbon dioxide and methane retrieved from GOSAT short-wavelength infrared spectra, *Atmos. Meas. Tech.*, 4, 1061–1076, doi:10.5194/amt-4-1061-2011, 2011.

Nakakita, E., Ikebuchi, S., Nakamura, T., Kanmuri, M., Okuda, M., Yamaji, A., and Takasao, T.: Short-term rainfall prediction method using a volume scanning radar and grid point value data from numerical weather prediction, *J. Geophys. Res.*, 101, 26181–26197, 1996.

Nakazawa, T., Machida, T., Sugawara, S., Murayama, S., Morimoto, S., Hashida, G., Honda, H., and Itoh, T.: Measurements of the stratospheric carbon dioxide concentration over Japan using a balloon-borne cryogenic sampler, *Geophys. Res. Lett.*, 22, 1229–1232, doi:10.1029/95GL01188, 1995.

Nakazawa, T., Ishizawa, M., Higuchi, K., and Trivett, N. B. A.: Two curve fitting methods applied to CO₂ flask data, *Environmetrics*, 8, 197–218, 1997a.

Nakazawa, T., Morimoto, S., Aoki, S., and Tanaka, M.: Temporal and spatial variations of the carbon isotopic ratio of atmospheric carbon dioxide in the western Pacific region, *J. Geophys. Res.*, 102, 1271–1285, 1997b.

**Validation of GOSAT
XCO₂ using aircraft
measurement**

M. Inoue et al.

Title Page

Abstract

Introduction

Conclusions

References

Tables

Figures

◀

▶

◀

▶

Back

Close

Full Screen / Esc

Printer-friendly Version

Interactive Discussion



- Nakazawa, T., Sugawara, S., Inoue, G., Machida, T., Maksyutov, S., and Mukai, H.: Aircraft measurements of the concentrations of CO₂, CH₄, N₂O, and CO and the carbon and oxygen isotopic ratios of CO₂ in the troposphere over Russia, *J. Geophys. Res.*, 102, 3843–3859, 1997c.
- 5 Niwa, Y., Machida, T., Sawa, Y., Matsueda, H., Schuck, T. J., Brenninkmeijer, C. A. M., Imasu, R., and Satoh, M.: Imposing strong constraints on tropical terrestrial CO₂ fluxes using passenger aircraft based measurements, *J. Geophys. Res.*, 117, D11303, doi:10.1029/2012JD017474, 2012.
- NOAA/ESRL Carbon Cycle Greenhouse Gases Aircraft Program, available at: <http://www.esrl.noaa.gov/gmd/ccgg/aircraft/index.html> (last access: January 2013), 2012.
- 10 Numaguti, A., Takahashi, M., Nakajima, T., and Sumi, A.: Development of CCSR/NIES atmospheric general circulation model, in: Reports of a New Program for Creative Basic Research Studies, CGER's Supercomputer. Monogr. Rep., 3, CGER, National Institute for Environmental Studies, Tsukuba, Japan, 1–48, 1997.
- 15 Ohyama, H., Morino, I., Nagahama, T., Machida, T., Suto, H., Oguma, H., Sawa, Y., Matsueda, H., Sugimoto, N., Nakane, H., and Nakagawa, K.: Column-averaged volume mixing ratio of CO₂ measured with ground-based Fourier transform spectrometer at Tsukuba, *J. Geophys. Res.*, 114, D18303, doi:10.1029/2008JD011465, 2009.
- Pales, J. C. and Keeling, C. D.: The concentration of atmospheric carbon dioxide in Hawaii, *J. Geophys. Res.*, 70, 6053–6076, doi:10.1029/JZ070i024p06053, 1965.
- 20 Pan, L. L. and Munchak, L. A.: Relationship of cloud top to the tropopause and jet structure from CALIPSO data, *J. Geophys. Res.*, 116, D12201, doi:10.1029/2010JD015462, 2011.
- Patra, P. K., Takigawa, M., Dutton, G. S., Uhse, K., Ishijima, K., Lintner, B. R., Miyazaki, K., and Elkins, J. W.: Transport mechanisms for synoptic, seasonal and interannual SF₆ variations and “age” of air in troposphere, *Atmos. Chem. Phys.*, 9, 1209–1225, doi:10.5194/acp-9-1209-2009, 2009.
- 25 Patra, P. K., Niwa, Y., Schuck, T. J., Brenninkmeijer, C. A. M., Machida, T., Matsueda, H., and Sawa, Y.: Carbon balance of South Asia constrained by passenger aircraft CO₂ measurements, *Atmos. Chem. Phys.*, 11, 4163–4175, doi:10.5194/acp-11-4163-2011, 2011.
- 30 Rayner, P. J. and O'Brien, D. M.: The utility of remotely sensed CO₂ concentration data in surface source inversions, *Geophys. Res. Lett.*, 28, 175–178, 2001.

**Validation of GOSAT
XCO₂ using aircraft
measurement**

M. Inoue et al.

Title Page

Abstract

Introduction

Conclusions

References

Tables

Figures

◀

▶

◀

▶

Back

Close

Full Screen / Esc

Printer-friendly Version

Interactive Discussion



Reuter, M., Buchwitz, M., Schneising, O., Heymann, J., Bovensmann, H., and Burrows, J. P.: A method for improved SCIAMACHY CO₂ retrieval in the presence of optically thin clouds, *Atmos. Meas. Tech.*, 3, 209–232, doi:10.5194/amt-3-209-2010, 2010.

Rodgers, C. D. and Connor, B. J.: Intercomparison of remote sounding instruments, *J. Geophys. Res.*, 108, 4116, doi:10.1029/2002JD002299, 2003.

Saito, R., Patra, P. K., Deutscher, N., Wunch, D., Ishijima, K., Sherlock, V., Blumenstock, T., Dohe, S., Griffith, D., Hase, F., Heikkinen, P., Kyrö, E., Macatangay, R., Mendonca, J., Messerschmidt, J., Morino, I., Notholt, J., Rettinger, M., Strong, K., Sussmann, R., and Warneke, T.: Technical Note: Latitude-time variations of atmospheric column-average dry air mole fractions of CO₂, CH₄ and N₂O, *Atmos. Chem. Phys.*, 12, 7767–7777, doi:10.5194/acp-12-7767-2012, 2012.

Saitoh, N., Imasu, R., Ota, Y., and Niwa, Y.: CO₂ retrieval algorithm for the thermal infrared spectra of the Greenhouse Gases Observing Satellite: potential of retrieving CO₂ vertical profile from high-resolution FTS sensor, *J. Geophys. Res.*, 114, D17305, doi:10.1029/2008JD011500, 2009.

Sawa, Y., Machida, T., and Matsueda, H.: Seasonal variations of CO₂ near the tropopause observed by commercial aircraft, *J. Geophys. Res.*, 113, D23301, doi:10.1029/2008JD010568, 2008.

Schneising, O., Buchwitz, M., Burrows, J. P., Bovensmann, H., Reuter, M., Notholt, J., Macatangay, R., and Warneke, T.: Three years of greenhouse gas column-averaged dry air mole fractions retrieved from satellite – Part 1: Carbon dioxide, *Atmos. Chem. Phys.*, 8, 3827–3853, doi:10.5194/acp-8-3827-2008, 2008.

Schneising, O., Bergamaschi, P., Bovensmann, H., Buchwitz, M., Burrows, J. P., Deutscher, N. M., Griffith, D. W. T., Heymann, J., Macatangay, R., Messerschmidt, J., Notholt, J., Rettinger, M., Reuter, M., Sussmann, R., Velasco, V. A., Warneke, T., Wennberg, P. O., and Wunch, D.: Atmospheric greenhouse gases retrieved from SCIAMACHY: comparison to ground-based FTS measurements and model results, *Atmos. Chem. Phys.*, 12, 1527–1540, doi:10.5194/acp-12-1527-2012, 2012.

Takagi, H., Saeki, T., Oda, T., Saito, M., Valsala, V., Belikov, D., Saito, R., Yoshida, Y., Morino, I., Uchino, O., Andres, R. J., Yokota, T., and Maksyutov, S.: On the Benefit of GOSAT Observations to the Estimation of Regional CO₂ Fluxes, *Sci. Online Lett. Atmos. (SOLA)*, 7, 161–164, doi:10.2151/sola.2011-041, 2011.

Validation of GOSAT XCO₂ using aircraft measurement

M. Inoue et al.

Title Page

Abstract

Introduction

Conclusions

References

Tables

Figures

◀

▶

◀

▶

Back

Close

Full Screen / Esc

Printer-friendly Version

Interactive Discussion

Tans, P. P., Conway, T., and Nakazawa, T.: Latitudinal distribution of the sources and sinks of atmospheric carbon dioxide derived from surface observations and an Atmospheric Transport Model, *J. Geophys. Res.*, 94, 5151–5172, 1989.

Uchino, O., Kikuchi, N., Sakai, T., Morino, I., Yoshida, Y., Nagai, T., Shimizu, A., Shibata, T., Yamazaki, A., Uchiyama, A., Kikuchi, N., Oshchepkov, S., Bril, A., and Yokota, T.: Influence of aerosols and thin cirrus clouds on the GOSAT-observed CO₂: a case study over Tsukuba, *Atmos. Chem. Phys.*, 12, 3393–3404, doi:10.5194/acp-12-3393-2012, 2012.

Washenfelder, R. A., Toon, G. C., Blavier, J.-F., Yang, Z., Allen, N. T., Wennberg, P. O., Vay, S. A., Matross, D. M., and Daube, B. C.: Carbon dioxide column abundances at the Wisconsin tall tower site, *J. Geophys. Res.*, 111, D22305, doi:10.1029/2006JD007154, 2006.

Watanabe, F., Uchino, O., Joo, Y., Aono, M., Higashijima, K., Hirano, Y., Tsuboi, K., and Suda, K.: Interannual variation of growth rate of atmospheric carbon dioxide concentration observed at the JMA's three monitoring stations, *J. Meteor. Soc. Jpn.*, 78, 673–682, 2000.

WMO: WMO Greenhouse Gas Bulletin, The State of Greenhouse Gases in the Atmosphere Using Global Observations through 2006, No. 3, World Meteorological Organization, 2007, available at: http://www.wmo.int/pages/prog/arep/gaw/ghg/ghgbull06_en.html (last access: January 2013), 2012.

WMO: WMO Greenhouse Gas Bulletin, The State of Greenhouse Gases in the Atmosphere Based on Global Observations through 2009, No. 6, World Meteorological Organization, 2010, available at: http://www.wmo.int/pages/prog/arep/gaw/ghg/ghgbull06_en.html (last access: January 2013), 2012.

Wunch, D., Toon, G. C., Wennberg, P. O., Wofsy, S. C., Stephens, B. B., Fischer, M. L., Uchino, O., Abshire, J. B., Bernath, P., Biraud, S. C., Blavier, J.-F. L., Boone, C., Bowman, K. P., Browell, E. V., Campos, T., Connor, B. J., Daube, B. C., Deutscher, N. M., Diao, M., Elkins, J. W., Gerbig, C., Gottlieb, E., Griffith, D. W. T., Hurst, D. F., Jiménez, R., Keppel-Aleks, G., Kort, E. A., Macatangay, R., Machida, T., Matsueda, H., Moore, F., Morino, I., Park, S., Robinson, J., Roehl, C. M., Sawa, Y., Sherlock, V., Sweeney, C., Tanaka, T., and Zondlo, M. A.: Calibration of the Total Carbon Column Observing Network using aircraft profile data, *Atmos. Meas. Tech.*, 3, 1351–1362, doi:10.5194/amt-3-1351-2010, 2010.

Wunch, D., Toon, G. C., Blavier, J.-F. L., Washenfelder, R. A., Notholt, J., Connor, B. J., Griffith, D. W. T., Sherlock, V., and Wennberg, P. O.: The total carbon column observing network, *Philos. T. Roy. Soc. A*, 369, 2087–2112, doi:10.1098/rsta.2010.0240, 2011.

Validation of GOSAT XCO₂ using aircraft measurement

M. Inoue et al.

Title Page

Abstract

Introduction

Conclusions

References

Tables

Figures

◀

▶

◀

▶

Back

Close

Full Screen / Esc

Printer-friendly Version

Interactive Discussion



Yang, Z., Washenfelder, R. A., Keppel-Aleks, G., Krakauer, N. Y., Randerson, J. T., Tans, P. P., Sweeney, C., and Wennberg, P. O.: New constraints on Northern Hemisphere growing season net flux, *Geophys. Res. Lett.*, 34, L12807, doi:10.1029/2007GL029742, 2007.

5 Yokota, T., Yoshida, Y., Eguchi, N., Ota, Y., Tanaka, T., Watanabe, H., and Maksyutov, S.: Global concentrations of CO₂ and CH₄ retrieved from GOSAT: first preliminary results, *Sci. Online Lett. Atmos. (SOLA)*, 5, 160–163, doi:10.2151/sola.2009-041, 2009.

Yoshida, Y., Oguma, H., Morino, I., Suto, H., Kuze, A., and Yokota, T.: Mountaintop observation of CO₂ absorption spectra using a short wavelength infrared Fourier transform spectrometer, *Appl. Optics*, 49, 71–79, 2010.

10 Yoshida, Y., Ota, Y., Eguchi, N., Kikuchi, N., Nobuta, K., Tran, H., Morino, I., and Yokota, T.: Retrieval algorithm for CO₂ and CH₄ column abundances from short-wavelength infrared spectral observations by the Greenhouse gases observing satellite, *Atmos. Meas. Tech.*, 4, 717–734, doi:10.5194/amt-4-717-2011, 2011.

15 Yoshida, Y., Kikuchi, N., Morino, I., Uchino, O., Oshchepkov, S., Bril, A., Saeki, T., Schutgens, N., Toon, G. C., Wunch, D., Roehl, C. M., Wennberg, P. O., Griffith, D. W. T., Deutscher, N. M., Warneke, T., Notholt, J., Robinson, J., Sherlock, V., Connor, B., Rettinger, M., Sussmann, R., Ahonen, P., Heikkinen, P., Kyrö, E., and Yokota, T.: Improvement of the retrieval algorithm for GOSAT SWIR XCO₂ and XCH₄ and their validation using TCCON data, *Atmos. Meas. Tech. Discuss.*, 6, 949–988, doi:10.5194/amtd-6-949-2013, 2013.

Table 1. Basic information for the aircraft measurement sites used for the GOSAT validation.

(a) CONTRAIL					
site code	latitude [° N]	longitude [° E]	elevation [m]	region	airport name
AMS	52.3	4.8	3	Amsterdam	Schiphol Airport
LHR	51.5	-0.5	24	London	Heathrow Airport
YVR	49.2	-123.2	4	Vancouver	Vancouver International Airport
CDG	49.0	2.5	119	Paris	Charles de Gaulle International Airport
MXP	45.6	8.7	24	Milan	Milan Malpensa International Airport
FCO	41.8	12.3	5	Rome	Fiumicino Airport
ICN	37.5	126.5	7	Incheon	Incheon International Airport
NRT	35.8	140.4	43	Narita	Narita International Airport
HND	35.6	139.8	6	Haneda	Tokyo International Airport
NGO	34.9	136.8	5	Nagoya	Chubu Centrair International Airport
KIX	34.4	135.2	0	Kansai	Kansai International Airport
DEL	28.6	77.1	237	Delhi	Indira Gandhi International Airport
TPE	25.1	121.2	32	Taipei	Taiwan Taoyuan International Airport
HNL	21.3	-157.9	4	Honolulu	Honolulu International Airport
MNL	14.5	121.0	23	Manila	Ninoy Aquino International Airport
BKK	13.7	100.7	2	Bangkok	Suvarnabhumi International Airport
GUM	13.5	144.8	91	Guam	Guam International Airport
SIN	1.4	104.0	7	Singapore	Singapore Changi International Airport
CGK	-6.1	106.7	10	Jakarta	Jakarta International Soekarno-Hatta Airport
SYD	-33.9	151.2	6	Sydney	Kingsford Smith Airport

(b) NOAA					
site code	latitude [° N]	longitude [° E]	elevation [m]	region	site name
PFA	65.1	-147.3	210	United States	Poker Flat, Alaska
BRM	54.3	-105.0	507	Canada	BERMS, Saskatchewan
ESP	49.6	-126.4	7	Canada	Estevan Point, British Columbia
DND	48.4	-97.8	464	United States	Dahlen, North Dakota
LEF	45.9	-90.3	472	United States	Park Falls, Wisconsin
NHA	43.0	-70.6	0	United States	Worcester, Massachusetts
WBI	41.7	-91.4	242	United States	West Branch, Iowa
THD	41.1	-124.2	107	United States	Trinidad Head, California
BNE	40.8	-97.2	466	United States	Beaver Crossing, Nebraska
CAR	40.4	-104.3	1740	United States	Briggsdale, Colorado
HIL	40.1	-87.9	202	United States	Homer, Illinois
AAO	40.1	-88.6	213	United States	Airborne Aerosol Observing, Illinois
CMA	38.8	-74.3	0	United States	Cape May, New Jersey
SGP	36.8	-97.5	314	United States	Southern Great Plains, Oklahoma
SCA	32.8	-79.6	0	United States	Charleston, South Carolina
TGC	27.7	-96.9	0	United States	Sinton, Texas
RTA	-21.3	-159.8	3	Cook Islands	Rarotonga

(c) NIES					
site code	latitude [° N]	longitude [° E]	elevation [m]	region	site name
YKT	62	130	136	Russia	Yakutsk
SRG	61	73	35	Russia	Surgut
NVS	55	83	143	Russia	Novosibirsk
SGM	35.1	139.3		Japan	Sagami-bay

**Validation of GOSAT
XCO₂ using aircraft
measurement**

M. Inoue et al.

Title Page

Abstract Introduction

Conclusions References

Tables Figures

◀ ▶

◀ ▶

Back Close

Full Screen / Esc

Printer-friendly Version

Interactive Discussion



Table 2. The average, maximum, minimum, and 1 standard deviation (1σ) of the differences between aircraft-based XCO_2 with and without the application of GOSAT column averaging kernels at each aircraft observation site.

site	number	average [ppm]	1σ [ppm]	maximum [ppm]	minimum [ppm]
AMS	10	0.041	0.071	0.109	-0.100
LHR	5	-0.073	0.088	0.023	-0.204
YVR	7	0.005	0.085	0.115	-0.165
CDG	5	0.173	0.070	0.247	0.083
MXP	2	0.031	0.015	0.042	0.020
FCO	2	0.141	0.000	0.141	0.141
ICN	2	0.033	0.011	0.041	0.025
NRT	225	-0.030	0.095	0.245	-0.360
HND	17	0.052	0.084	0.188	-0.085
NGO	37	-0.056	0.077	0.127	-0.245
KIX	21	-0.069	0.091	0.090	-0.197
DEL	6	0.021	0.035	0.062	-0.026
TPE	1	-0.058	-	-0.058	-0.058
HNL	35	-0.008	0.088	0.174	-0.207
MNL	2	-0.019	0.109	0.058	-0.096
BKK	33	0.004	0.067	0.136	-0.133
GUM	0	-	-	-	-
SIN	13	-0.050	0.095	0.070	-0.249
CGK	10	-0.043	0.041	0.024	-0.114
SYD	52	-0.033	0.074	0.062	-0.229
PFA	0	-	-	-	-
BRM	1	-0.010	-	-0.010	-0.010
ESP	0	-	-	-	-
DND	7	0.039	0.060	0.140	-0.045
LEF	17	0.035	0.067	0.157	-0.132
NHA	17	0.007	0.108	0.252	-0.105
WBI	12	-0.037	0.055	0.084	-0.109
THD	3	0.009	0.035	0.041	-0.028
BNE	5	0.034	0.030	0.066	-0.011
CAR	20	-0.014	0.078	0.124	-0.223
HIL	17	-0.049	0.069	0.101	-0.135
AAO	29	0.002	0.074	0.122	-0.127
CMA	1	-0.039	-	-0.039	-0.039
SGP	25	-0.065	0.057	0.067	-0.142
SCA	9	-0.057	0.060	0.031	-0.157
TGC	7	-0.039	0.087	0.044	-0.210
RTA	5	-0.094	0.067	-0.017	-0.184
YKT	0	-	-	-	-
SRG	0	-	-	-	-
NVS	0	-	-	-	-
SGM	3	0.090	0.147	0.240	-0.055
All data	663	-0.021	0.089	0.252	-0.360

**Validation of GOSAT
 XCO_2 using aircraft
measurement**

M. Inoue et al.

Title Page

Abstract Introduction

Conclusions References

Tables Figures

◀ ▶

◀ ▶

Back Close

Full Screen / Esc

Printer-friendly Version

Interactive Discussion



Validation of GOSAT XCO₂ using aircraft measurement

M. Inoue et al.

Title Page

Abstract

Introduction

Conclusions

References

Tables

Figures

◀

▶

◀

▶

Back

Close

Full Screen / Esc

Printer-friendly Version

Interactive Discussion



Table 3. The average and 1 standard deviation (1σ) of the differences of aircraft-based XCO₂ calculated by using ACTM, a priori profiles of TCCON, and a priori profiles as in the GOSAT retrieval system in the stratosphere and mesosphere, at each aircraft observation site.

aircraft site (TCCON site)	number	ACTM-TCCON prior		ACTM-GOSAT prior	
		average [ppm]	1σ [ppm]	average [ppm]	1σ [ppm]
LEF (Park Falls)	11	-0.311	0.076	-0.099	0.759
SGP (Lamont)	25	-0.176	0.083	0.461	0.337
NRT (Tsukuba)	60	-0.115	0.083	0.037	0.082
SYD (Wollongong)	20	-0.198	0.060	0.094	0.071
All data	116	-0.161	0.098	0.125	0.334

Table 4. The average and 1 standard deviation (1σ) of the differences between GOSAT XCO₂ and aircraft-based XCO₂ at each site. The GOSAT data were retrieved over (a) land and (b) ocean regions within $\pm 2^\circ$ and $\pm 5^\circ$ latitude/longitude boxes centered at each aircraft observation site.

(a) Land site	$\pm 2^\circ$			$\pm 5^\circ$		
	number	average [ppm]	1σ [ppm]	number	average [ppm]	1σ [ppm]
NRT	25	-0.212	2.646	40	-0.266	2.448
LHR	0	-	1.733	3	-3.173	1.733
YVR	0	-	2.232	6	-1.039	2.232
MXP	0	-	1.943	2	-0.182	1.943
ICN	1	0.331	-	1	0.331	-
NGO	6	0.093	3.732	11	0.366	2.817
KIX	1	-1.076	-	4	-1.299	2.781
TPE	0	-	-	1	4.705	-
BKK	0	-	-	4	-3.832	4.028
SYD	2	-0.630	1.172	9	-1.863	1.922
DND	0	-	-	1	-0.779	-
LEF	1	-2.621	-	5	-2.886	1.963
NHA	1	-1.705	-	7	0.061	1.852
WBI	1	-5.608	-	10	-1.417	2.301
THD	1	-1.978	-	1	-1.978	-
BNE	0	-	-	2	-3.198	0.754
CAR	1	-2.601	-	9	-2.500	2.667
HIL	7	-1.369	1.752	11	-1.465	1.644
AAO	6	-0.488	1.362	20	-0.331	2.267
SGP	9	-2.662	1.677	16	-2.656	1.876
SCA	6	-0.919	2.320	7	-0.090	1.192
TGC	1	2.470	-	5	-0.924	2.517
SGM	2	3.630	3.739	2	3.630	3.739
All data	71	-0.754	2.566	177	-1.006	2.510

Validation of GOSAT XCO₂ using aircraft measurement

M. Inoue et al.

Title Page

Abstract Introduction

Conclusions References

Tables Figures

◀ ▶

◀ ▶

Back Close

Full Screen / Esc

Printer-friendly Version

Interactive Discussion



Validation of GOSAT XCO₂ using aircraft measurement

M. Inoue et al.

Table 5. The average and 1 standard deviation (1σ) of the differences between GOSAT XCO₂ and aircraft-based XCO₂ for all sites by curve fitting.

$\pm 2^\circ$			
	number	average [ppm]	1σ [ppm]
Land	2313	-1.56	2.36
Ocean	85	-1.52	2.02
$\pm 5^\circ$			
	number	average [ppm]	1σ [ppm]
Land	11 146	-1.81	2.37
Ocean	708	-1.73	2.35

[Title Page](#)
[Abstract](#)
[Introduction](#)
[Conclusions](#)
[References](#)
[Tables](#)
[Figures](#)
[◀](#)
[▶](#)
[◀](#)
[▶](#)
[Back](#)
[Close](#)
[Full Screen / Esc](#)
[Printer-friendly Version](#)
[Interactive Discussion](#)


Validation of GOSAT
XCO₂ using aircraft
measurement

M. Inoue et al.

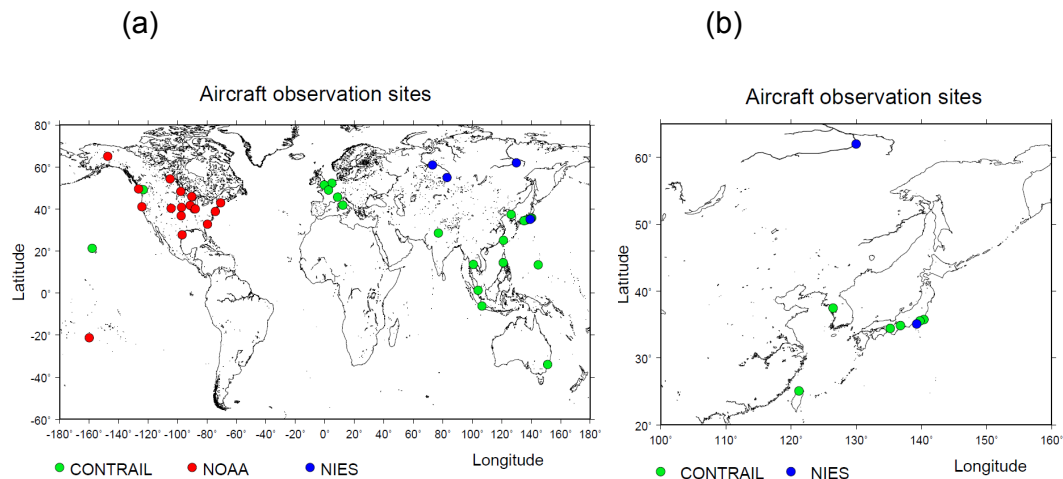


Fig. 1. (a) Global distribution of aircraft observation sites used for GOSAT validation. The East Asian region is expanded in (b).

[Title Page](#)[Abstract](#)[Introduction](#)[Conclusions](#)[References](#)[Tables](#)[Figures](#)[◀](#)[▶](#)[◀](#)[▶](#)[Back](#)[Close](#)[Full Screen / Esc](#)[Printer-friendly Version](#)[Interactive Discussion](#)

Validation of GOSAT
XCO₂ using aircraft
measurement

M. Inoue et al.

Title Page

Abstract

Introduction

Conclusions

References

Tables

Figures

◀

▶

◀

▶

Back

Close

Full Screen / Esc

Printer-friendly Version

Interactive Discussion

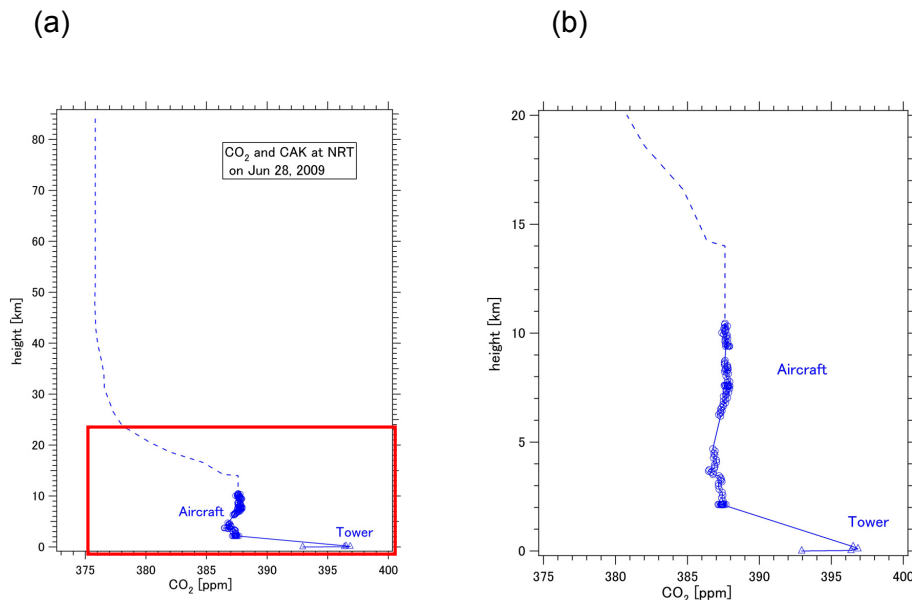


Fig. 2. An example of CO₂ profiles constructed over Narita (Japan). **(a)** High-altitude profile. The rectangular area is expanded in **(b)**. The open circles and triangles represent aircraft data and tower data, respectively. The solid and dashed lines show the observed and assumed CO₂ profiles, respectively. See text for more details.

Validation of GOSAT
XCO₂ using aircraft
measurement

M. Inoue et al.

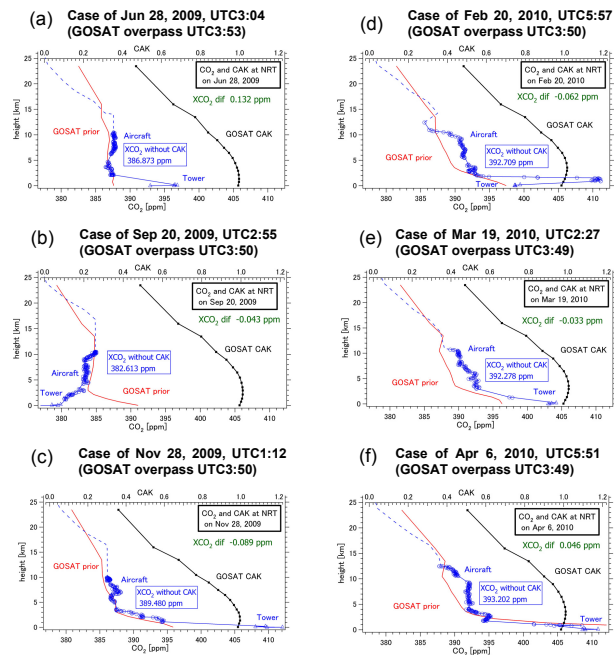


Fig. 3. Vertical profiles of CO₂ and GOSAT CAK over Narita on (a) 28 June 2009, (b) 20 September 2009, (c) 28 November 2009, (d) 20 February 2010, (e) 19 March 2010, and (f) 6 April 2010. The blue lines show the profiles of observation data, including aircraft measurements. The red lines show the GOSAT a priori profiles. The black lines are GOSAT CAKs. Aircraft-based XCO₂ without the application of GOSAT CAK, and the differences between aircraft-based XCO₂ with and without the application of GOSAT CAK are indicated by blue and green letters, respectively.

Title Page

Abstract

Introduction

Conclusions

References

Tables

Figures

◀

▶

◀

▶

Back

Close

Full Screen / Esc

Printer-friendly Version

Interactive Discussion

Validation of GOSAT
XCO₂ using aircraft
measurement

M. Inoue et al.

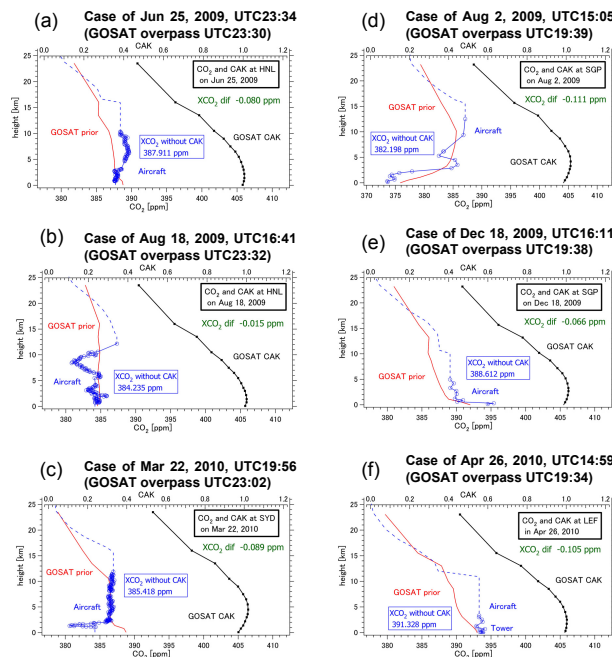


Fig. 4. Vertical profiles of CO₂ and GOSAT CAK over Honolulu on **(a)** 25 June 2009 and **(b)** 18 August 2009, over **(c)** Sydney on 22 March 2010, over the Southern Great Plains on **(d)** 2 August 2009 and **(e)** 18 December 2009, and over **(f)** Park Falls on 26 April 2010. The blue lines show observation data, including aircraft measurements. The red lines show the GOSAT a priori profiles. The black lines are GOSAT CAKs. Aircraft-based XCO₂ without the application of GOSAT CAK, and the differences between aircraft-based XCO₂ with and without the application of GOSAT CAK are indicated by blue and green letters, respectively.

Title Page

Abstract

Introduction

Conclusions

References

Tables

Figures

◀

▶

◀

▶

Back

Close

Full Screen / Esc

Printer-friendly Version

Interactive Discussion



Validation of GOSAT XCO₂ using aircraft measurement

M. Inoue et al.

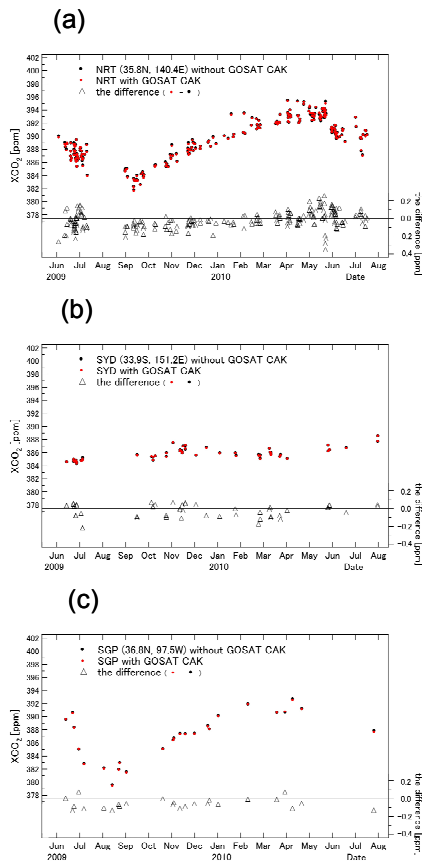


Fig. 5. Temporal variations of XCO₂ with and without CAK in (a) Narita, (b) Sydney, (c) the Southern Great Plains, (d) Bangkok, (e) Honolulu, and (f) Briggsdale. Red and black closed circles indicate XCO₂ with and without the application of CAK, respectively. Open triangles denote the differences between XCO₂ with CAK and without CAK.

[Title Page](#)
[Abstract](#)
[Introduction](#)
[Conclusions](#)
[References](#)
[Tables](#)
[Figures](#)
[Back](#)
[Close](#)
[Full Screen / Esc](#)
[Printer-friendly Version](#)
[Interactive Discussion](#)

Validation of GOSAT XCO₂ using aircraft measurement

M. Inoue et al.

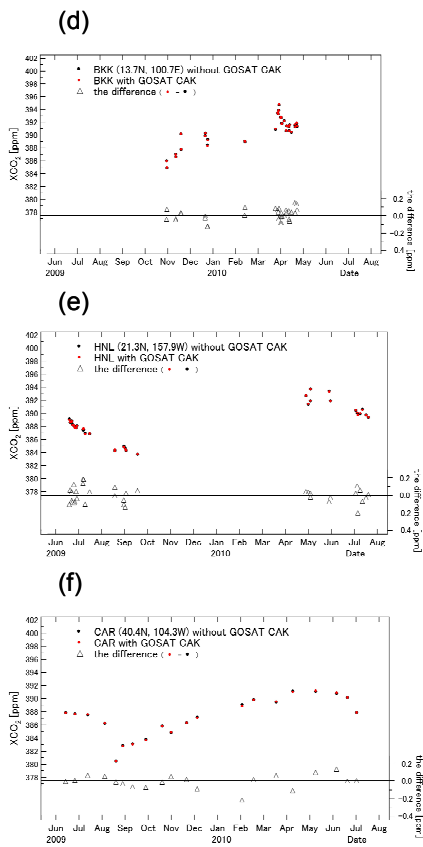


Fig. 5. Continued.

Title Page

Abstract

Introduction

Conclusions

References

Tables

Figures

◀

▶

◀

▶

Back

Close

Full Screen / Esc

Printer-friendly Version

Interactive Discussion



Validation of GOSAT XCO₂ using aircraft measurement

M. Inoue et al.

Title Page

Abstract

Introduction

Conclusions

References

Tables

Figures

◀

▶

◀

▶

Back

Close

Full Screen / Esc

Printer-friendly Version

Interactive Discussion

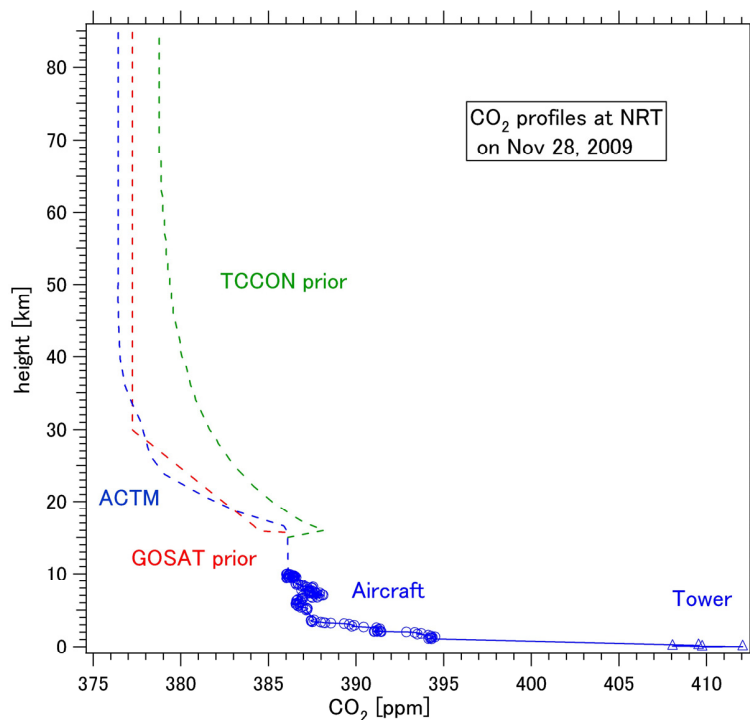


Fig. 6. Vertical profiles of CO₂ over Narita on 28 November 2009. Blue, red, and green dashed lines above the tropopause indicate profiles by ACTM, a priori as in the GOSAT retrieval, and a priori of TCCON, respectively. The blue solid lines show observation data, including aircraft measurements.

Validation of GOSAT XCO₂ using aircraft measurement

M. Inoue et al.

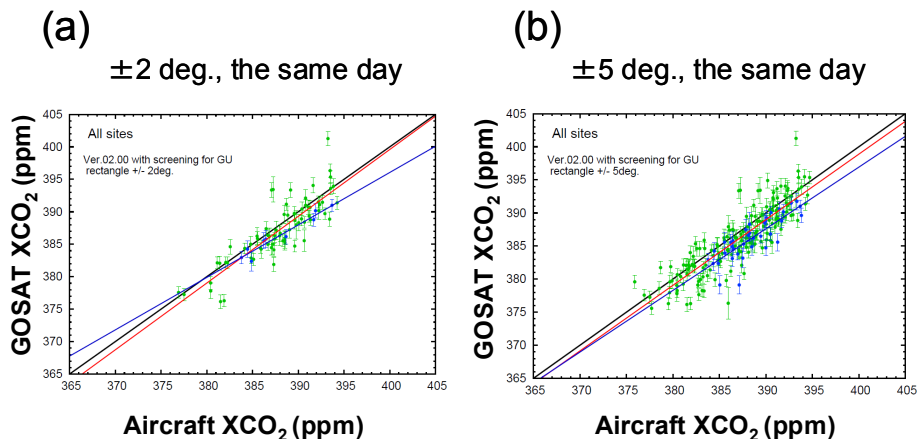


Fig. 7. Scatter diagrams between GOSAT XCO₂ observed within **(a)** $\pm 2^\circ$ and **(b)** $\pm 5^\circ$ latitude/longitude boxes centered at each aircraft observation site and aircraft-based XCO₂ with the application of CAK measured on a GOSAT overpass day. Green and blue dots indicate GOSAT XCO₂ obtained over land and ocean regions, respectively. Red and blue lines denote the regression lines with statistical significance at the 95 % level over land and ocean regions, respectively. The one-to-one lines are plotted as black lines.

Title Page

Abstract

Introduction

Conclusions

References

Tables

Figures

◀

▶

◀

▶

Back

Close

Full Screen / Esc

Printer-friendly Version

Interactive Discussion



Validation of GOSAT
XCO₂ using aircraft
measurement

M. Inoue et al.

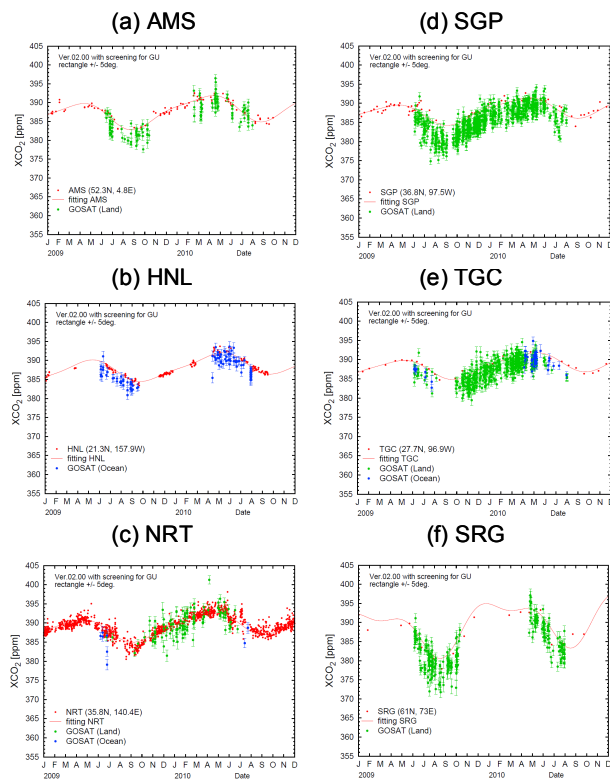


Fig. 8. Temporal variations of aircraft-based XCO₂ and GOSAT XCO₂ observed within ±5° latitude/longitude boxes centered at each aircraft site for **(a)** Amsterdam, **(b)** Honolulu, **(c)** Narita, **(d)** the Southern Great Plains, **(e)** Sinton, and **(f)** Surgut. Green and blue dots show the XCO₂ data over land and ocean regions, respectively. Red dots and lines indicate the aircraft-based XCO₂ and fitted curves based on their data, respectively.

Validation of GOSAT
XCO₂ using aircraft
measurement

M. Inoue et al.

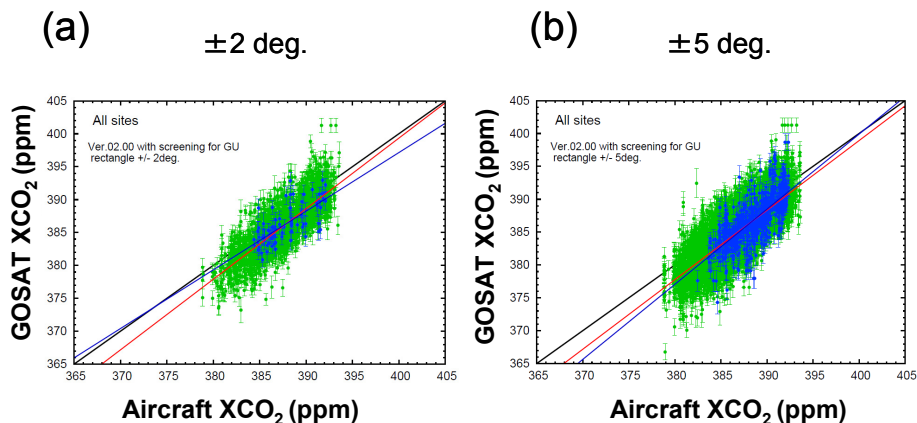


Fig. 9. Scatter diagrams between GOSAT XCO₂ observed within (a) $\pm 2^\circ$ and (b) $\pm 5^\circ$ latitude/longitude boxes centered at each aircraft observation site and the aircraft-based XCO₂ (estimate values obtained by a curve fitting method). Green and blue dots indicate XCO₂ obtained over land and ocean regions, respectively. Red and blue lines denote the regression lines with statistical significance at the 95 % level over land and ocean regions, respectively. The one-to-one lines are plotted as black lines.

Title Page

Abstract

Introduction

Conclusions

References

Tables

Figures

◀

▶

◀

▶

Back

Close

Full Screen / Esc

Printer-friendly Version

Interactive Discussion

